Supporting Information

Engineering CoO/Co_3O_4 Heterostructures Coupled with Adjacent Fe Single Atoms to Boost Tandem Electrocatalytic Nitrate Reduction for High-Efficiency Ammonia Production

Shan Wang, Zhiman Bai,* Kun Huang, Lingfan Wang, Fusheng Wang, Tongtong Jiang, Mingzai Wu*

S. Wang, Z. Bai, K. Huang, L. Wang, F. Wang, T. Jiang, Prof. M. Wu
Key Laboratory of Photoelectric Conversion Energy Materials and Devices of Anhui Province, School of Materials Science and Engineering, Anhui university, Hefei 230601, P. R. China
E-mail: wumz@ahu.edu.cn, baizhiman@ahu.edu.cn

Experimental section

Materials and chemicals

Zinc nitrate hexahydrate ($Zn(NO_3)_2·6H_2O$, 99%, Aladdin), 2-methylimidazole ($C_4H_6N_2$, 98%, Aladdin), Fe (III) acetylacetonate ($Fe(acac)_3$, 98%, Aladdin), cobalt nitrate hexahydrate ($Co(NO_3)_2·6H_2O$, 99%, Aladdin), Sodium borohydride ($NaBH_4$, 98%, Aladdin), methanol (CH_3OH, 99.9%, Aladdin), ethanol (C_2H_5OH, 99.9%, Aladdin), Sodium hypochlorite solution (NaClO, 6-14%, Aladdin), Sodium salicylate ($C_7H_5O_3Na$, 99.5%, Aladdin), Sodium nitroferricyanide dehydrate ($C_5FeN_6Na_2O$, 99%, Adamas-beta), sodium hydroxide (NaOH, ≥ 96.0%, Aladdin), ammonium sulfate ($(NH_4)_2SO_4$, 98.5%, Aladdin), Phosphoric acid (H_3PO_4, 98%, Damao), N-(1-naphthyl) ethyldiamine dihydrochloride (98%, Aladdin) and sulfonamide (99%, Aladdin), ^{14}N-NH_4Cl (99%, Aladdin), ^{15}N-NH_4Cl (> 99 atom%,), sodium nitrate-^{14}N ($Na^{14}NO_3$, 98.5%, Aladdin), sodium nitrate-^{15}N ($Na^{15}NO_3$,^{15}N ≥ 99 at%, 98.5%, Aladdin), maleic acid ($C_4H_4O_4$, ≥99.0%, Aladdin), deuterium oxide (D_2O, 99 at% D, Aladdin).

All the chemicals and solvents were reagent grade and used without further purification. Deionized water was used in all experiments.

Synthesis of FeSA NC and NC

$Zn(NO_3)_2·6H_2O$ (891mg, 3 mmol) and $Fe(acac)_3$ (107mg, 0.2 mmol) were simultaneously dissolved in 30 mL methanol. This solution was then added rapidly to a solution of 2-methylimidazole (1.97g, 24 mmol) in 30 mL methanol, and the resulting solution was stirred for 1 h at room temperature. Then, the solution was transferred into a Teflon-lined stainless-steel autoclave and the reaction was continued for 4 h at 120 °C. Subsequently, the Fe-ZIF-8 nanocrystal was collected by centrifugation, washed three times with methanol, and dried overnight in vacuum oven at 60 °C. The Fe-ZIF-8 powder was placed in a tube furnace, and calcinated at 950 °C for 2 h with a heating rate of 5 °C min^{-1}. Finally, FeSA NC was obtained after the sample was cooled to room temperature. The synthesis procedure for NC was identical to that of FeSA NC, except that $Fe(acac)_3$ was not added.

Synthesis of FeSA@CoO/Co_3O_4 NC and CoO/Co_3O_4 NC

160 mg of FeSA NC was dispersed in 20 mL of ethanol followed by the sonication for 30 min. Then, 5 mL of an aqueous solution containing 45 mg of $Co(NO_3)_2 \cdot 6H_2O$ was added to the aforementioned suspension under vigorous stirring for 1 h in an ice water bath. Thereafter, 40 mL of a freshly prepared ice-cold aqueous solution containing 100 mg $NaBH_4$ was added dropwise to the aforementioned suspension, with subsequent stirring maintained for 1 h. The as-obtained precipitate was collected by filtration and washed with deionized water five times. Finally, FeSA@CoO/Co_3O_4 NC was obtained after dried overnight at 60 °C in a vacuum oven. As a control sample, the preparation procedure of CoO/Co_3O_4 NC was the same as that of FeSA@CoO/Co_3O_4 NC, except with the addition of NC instead of FeSA NC.

The preparation of working electrode

Typically, 5 mg of the catalyst was dispersed in 960 μL of a water/ethanol mixed solution with a volume ratio of 3:1 ($V_{water}/V_{ethanol}$ = 3/1), followed by the addition of 40 μL of Nafion solution. Subsequently, the mixed suspension was sonicated to form a homogeneous catalyst ink. 50 μL of the catalyst ink was dripped onto carbon paper to get working electrode (the catalyst loading is 0.25 mg cm^{-2}).

Assembly of the Zn-NO_3^- battery

The electrochemical performance of hybrid liquid Zn-NO_3^- battery in a two-electrode system was determined in an H-type cell. A typical H-type cell contains 30 mL cathode electrolyte (5 M NaOH + 0.1 M $NaNO_3$) and 30 mL anode electrolyte (5 M NaOH), separated by a bipolar membrane. All battery data were recorded in CHI 760e electrochemical workstation.

Material characterization

Powder X-ray diffraction (XRD) patterns were recorded on a Philips X'Pert PRO SUPER X-ray diffractometer equipped with graphite-monochromated Cu Kα radiation (λ= 1.54056 Å). X-ray photoelectron spectroscopy (XPS) measurement was carried out on a Escalab 250Xi system using a monochromatic Al Ka source (1,486.6 eV) for the analysis of the surface chemical property. The electron paramagnetic resonance (EPR) measurements of DMPO-H were carried out at Bruker EMX plus 10/12 (equipped with

Oxford ESR 910 Liquid Helium cryostat). The ultraviolet-visible (UV-Vis) absorbance spectra were collected on Shimadzu UV-3900 spectrophotometer. The isotope labeling experiments were measured using ^{1}H-NMR measurement (JNM-ECZ400R). The morphology and structure observations of samples were conducted with TEM and HRTEM on JEOL field emission electron microscopy. Atomic structures of samples were observed through HAADF-STEM on a JEOL JEM-ARF200F (200 kV) with a spherical aberration corrector. The X-ray absorption near-edge structure (XANES) spectra and extended X-ray absorption fine structure (EXAFS) spectra at Fe K-edge and Co K-edge were performed at BL11B beamline of Shanghai Synchrotron Radiation Facility and the table XAFS-500A. The reaction intermediate information was studied by in situ Fourier-transform infrared (FTIR) Spectroscopy (Bruker INVENIO S, Germany).

Electrochemical measurements

The electrochemical measurements were conducted in a single-chamber electrolytic cell of a standard three-electrode system. The catalysts modified carbon fiber paper (1 cm^2), Ag/AgCl (KCl, 3.5 M), and Pt slice were served as working, reference, and counter electrode, respectively. The electrolyte was 30 mL of 0.5 M Na_2SO_4 aqueous solution containing 0.1 M $NaNO_3$. All potentials were recorded against a reversible hydrogen electrode (RHE). Liner sweep voltammetry (LSV) curves were collected at a scan rate of 10 mV s^{-1}. The potentiostatic tests were tested at different potentials for 1 h. The faraday efficiency (FE) and NH_3 yield rate were measured by chronoamperometry, and each measurement was repeated three times independently to ensure reliability. The corresponding values represent the averages of three independent replicate experiments, and the error bars represents the standard deviation of the three measurements. In the non-Faradaic voltage region, the electrochemical active surface area (ECSA) was assessed using the double-layer capacitances (C_{dl}) by evaluated using cyclic voltammetry curves at different scan rates ranging from 20 to 100 mV s^{-1}. By plotting the relationship between the current density and the scan rate at a specific potential in the CV curve, a straight line can be obtained. The slope of the straight line was defined as the C_{dl}. Electrochemical impedance

spectroscopy (EIS) was collected at the frequency range of 100 kHz to 0.01 Hz with an amplitude of 10 mV.

Determination of ion concentration

The UV-Vis spectrophotometer was used to detect the ion concentration of pre- and post-test electrolytes after diluting to appropriate concentration to match the range of calibration curves. The specific detection methods are as follow:

Determination of nitrite-N

A mixture of p-aminobenzenesulfonamide (4 g), N-(1-Naphthyl)-ethylenediamine dihydrochloride (0.2 g), ultrapure water (50 mL) and phosphoric acid (10 mL, ρ = 1.70 g/mL) was used as a color reagent. A certain amount of electrolyte was taken out from the electrolytic cell and diluted to 5 mL to detection range. Next, 0.1 mL color reagent was added into the aforementioned 5 mL solution and mixed well, standing for 20 minutes. Then, the absorbance intensity was recorded at a wavelength of 540 nm. The concentration-absorbance curve was calibrated using a series of standard sodium nitrite solutions.

Detection of ammonium-N

Determination of NH_3 concentration with indophenol blue method.[1] After the electroreduction process, a certain amount of electrolyte was taken out from the electrolytic cell and diluted to the detection range. Then, NaOH (0.4 g), sodium citrate (1 g), ultrapure water (20 mL) and salicylic acid (1 g) were added into the aforementioned solution, followed by the addition of 1 mL of 0.05 M NaClO and 0.2 mL of $C_5FeN_6Na_2O$ (1 wt%). After standing in darkness for 1 h, the absorption spectra were measured using a UV-Vis spectrophotometer. The concentration of indophenol blue was determined using absorbance at the wavelength of 650 nm. The concentration-absorbance curve was calibrated using standard $(NH_4)_2SO_4$ solution with a series of concentrations.

Isotope labeling experiments

$Na^{15}NO_3$ was used as the feeding N-source to perform the isotopic labeling nitrate reduction experiments to clarify the source of ammonia. 0.5 M Na_2SO_4 was used as

electrolyte with a concentration of 0.1M $Na^{15}NO_3^-$ was taken out, and quantified by the 1H-Nuclear Magnetic Resonance (NMR) spectroscopy. For quantification, a series of standard solutions and plotted the standard curve were prepared. First, a series of $^{15}NH_4^+$ solutions with known concentration were prepared in 0.5 M Na_2SO_4 as standards; Second, 30 mL of the $^{15}NH_4^+$standard solution with different concentration was mixed with 50 ppm maleic acid; Third, 50 μL deuterium oxide (D_2O) was added in 0.5 mL above mixed solution for the NMR detection; Fourth, the calibration was achieved using the peak area ratio between $^{15}NH_4^+$ and maleic acid because the $^{15}NH_4^+$ concentration and area ratio were positively correlated. Similarly, the amount of $^{14}NH_4^+$ was quantified by this method when $Na^{14}NO_3$ was used as the feeding N-source.

***H detection using DMPO**

For the *H trapping experiment, the electrolyte was set as 20 mL, and the cathode area was set as 1 × 1 cm^2 to ensure enough *H were generated. The reduce potential was set as −1.2 V (*vs*. RHE), 50 μL electrolyte was extracted and mixed with 10 μL DMPO after 10min. The mixture was transferred to capillary for detection. The data was obtained after removing the peaks of impurity.

In situ FTIR measurements

In situ Fourier-transform infrared (FTIR) spectroscopy measurements were performed using a Bruker INVENIO S spectrometer, with applied potential modulated by a CHI 760E electrochemical workstation. For the characterization, the prepared catalyst was deposited onto a carbon paper support with a geometric area of 1 × 1 cm^2. A three-electrode electrochemical cell was employed, utilizing an Ag/AgCl reference electrode and a platinum wire counter electrode. The electrolyte consisted of a mixed solution of 0.5 M Na_2SO_4 and 0.1 M $NaNO_3$.

Calculation of the yield, conversion rate, selectivity, and Faradaic efficiency

The yield was calculated by the following equation:

$$Yield_{NH3} = (C_{NH3} \times V)/(M_{NH3} \times t \times m)$$

The Faradaic efficiency was calculated according to the following equation:

$$Faradaic\ efficiency = \frac{8F \times C_{NH3} \times V}{M_{NH3} \times Q} \times 100\%$$

where C_{NH3} is the mass concentration of ammonia, V is the volume of electrolyte in the cathode compartment, M_{NH3} is the molar mass of ammonia, t is the reaction time, S is the area of the working electrode, F is the Faradaic constant (96485 C/mol) and Q is the total transferred electricity.

DFT calculations

First-principles calculations were performed using the Vienna Ab initio Simulation Package (VASP).[2,3] The exchange-correlation energy was treated using the generalized gradient approximation (GGA) in the form proposed by Perdew, Burke, and Ernzerhof (PBE).[4] The projector augmented wave (PAW) method was adopted to describe the interaction between core and valence electrons.[5] All DFT calculations were performed with a cut-off energy of 400 eV, and the $2 \times 2 \times 1$ Gamma centered Monkhorst-Pack grids k-points were selected to sample the Brillouin zone integration. The electronic and ionic convergence criteria were set to 1×10^{-5} eV and 0.02 eV $Å^{-1}$, respectively. To account for van der Waals (vdW) interactions, the DFT-D3 dispersion correction scheme was applied.[6]

In this study, the computational hydrogen electrode (CHE) model was employed to evaluate the Gibbs free energy change (ΔG) associated with the proton-coupled electron transfer (PCET) step. In the CHE framework, the chemical potential of a proton-electron pair is approximated by half the chemical potential of an H_2 molecule. The Gibbs free energy change was calculated using the following equation:

$$\Delta G = \Delta E + \Delta ZPE - T\Delta S,$$

In this equation, ΔE denotes the electronic energy difference between the initial and final states of the PCET step. ΔZPE corresponds to the difference in zero-point energy, while $T\Delta S$ accounts for the entropy change, where T is the absolute temperature (typically 298.15 K).

Supporting Fig.s

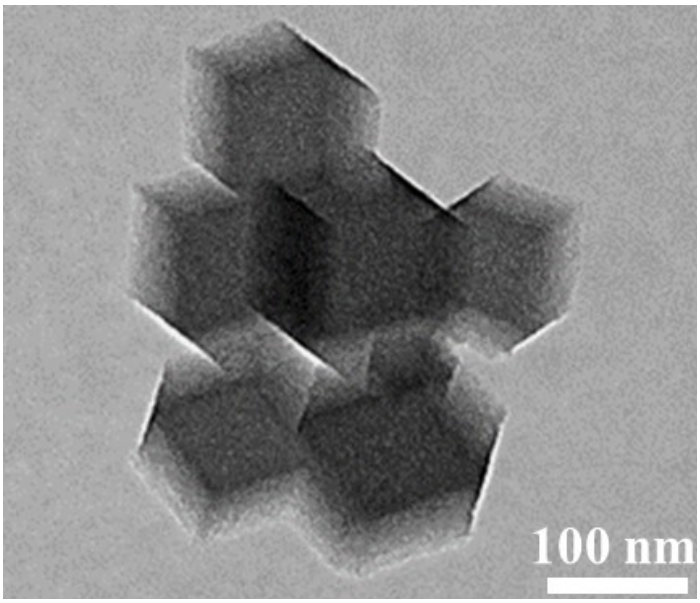

Fig. S1. TEM image of FeSA NC.

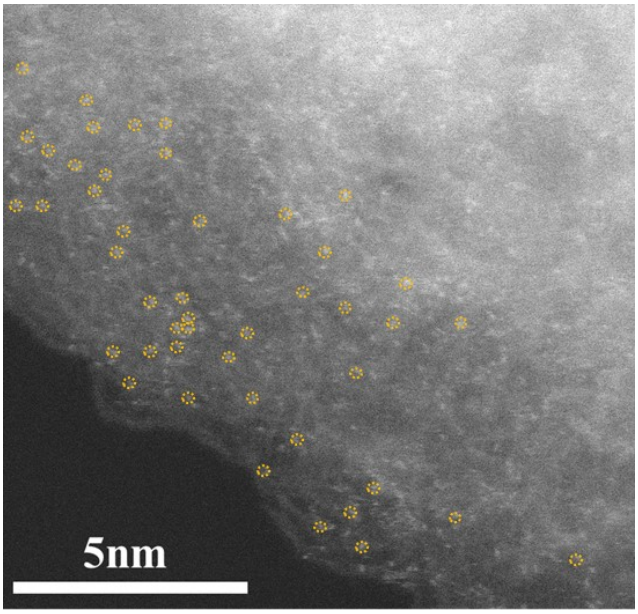

Fig. S2. Aberration-corrected HAADF-STEM image of FeSA NC.

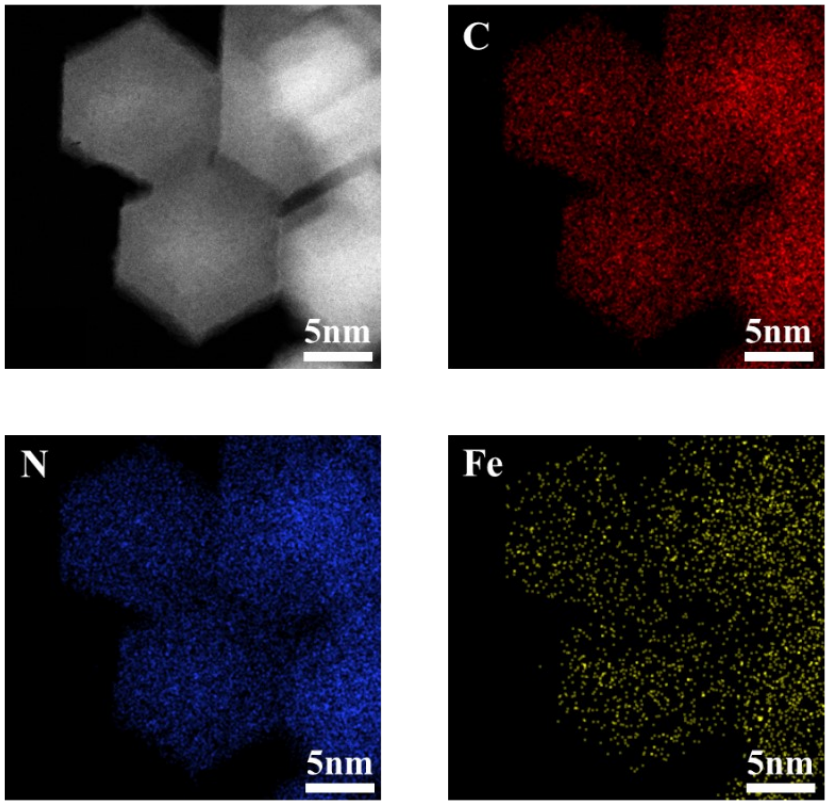

Fig. S3. HAADF-STEM image and corresponding EDS elemental mapping of FeSA NC.

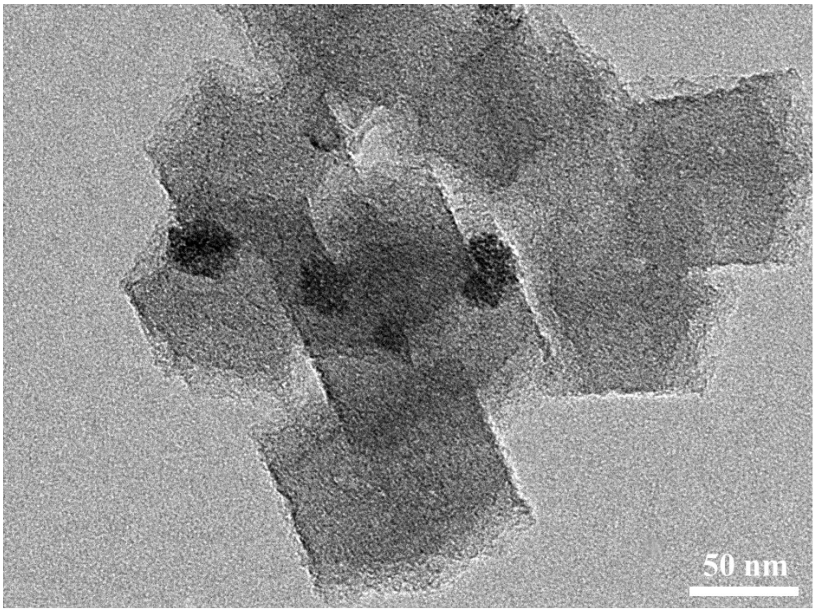

Fig. S4. TEM image of CoO/Co_3O_4 NC.

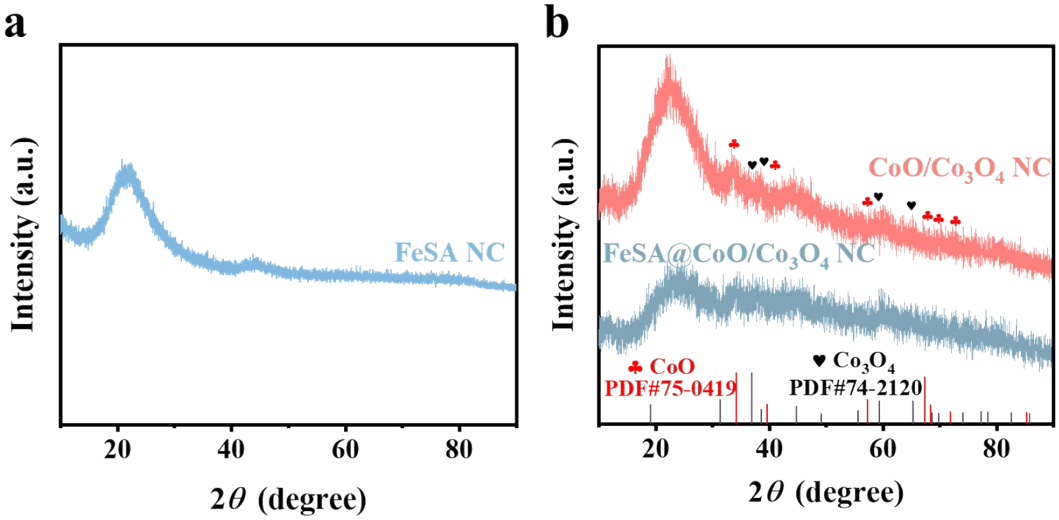

Fig. S5. XRD patterns of a) FeSA NC, and b) CoO/Co_3O_4 NC and $FeSA@CoO/Co_3O_4$ NC.

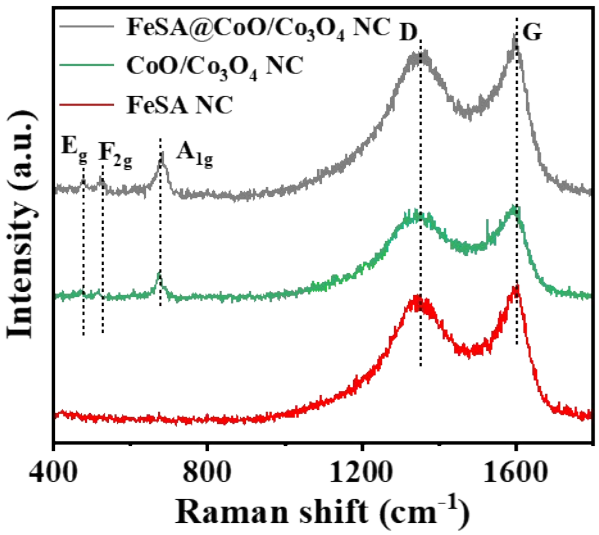

Fig. S6. Raman spectra of FeSA@CoO/Co_3O_4 NC, CoO/Co_3O_4 NC, and FeSA NC.

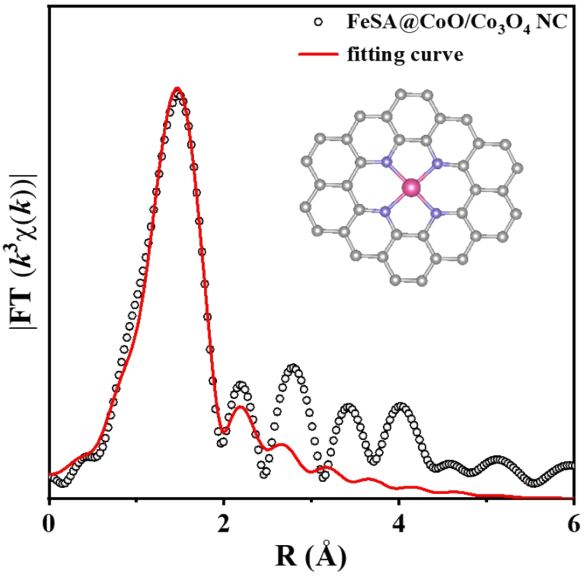

Fig. S7. Fitting results of the EXAFS spectrum of FeSA@CoO/Co_3O_4 NC at R space.

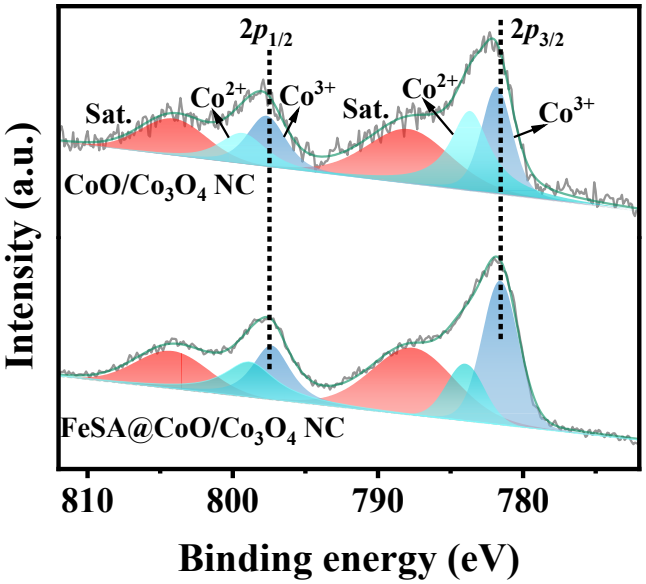

Fig. S8. Co 2p XPS spectra of FeSA@CoO/Co_3O_4 NC and CoO/Co_3O_4 NC.

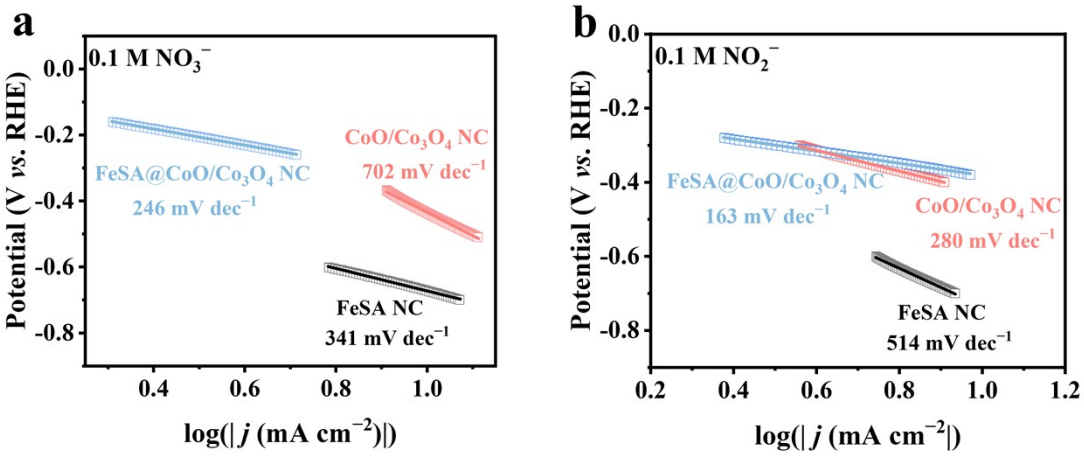

Fig. S9. Tafel slopes of FeSA NC, CoO/Co_3O_4 NC, and $FeSA@CoO/Co_3O_4$ NC in 0.5 M Na_2SO_4 aqueous containing a) 0.1 M NO_3^- and b) 0.1 M NO_2^-.

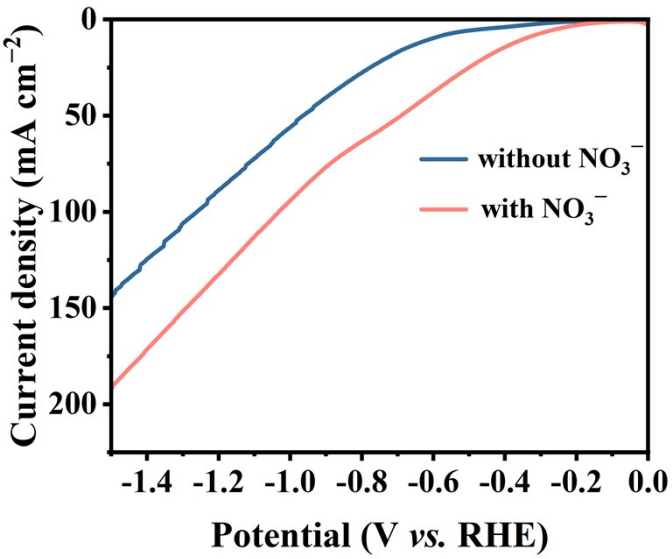

Fig. S10. LSV curve of FeSA@CoO/Co_3O_4 NC in 0.5 M Na_2SO_4 electrolyte with or without NO_3^-.

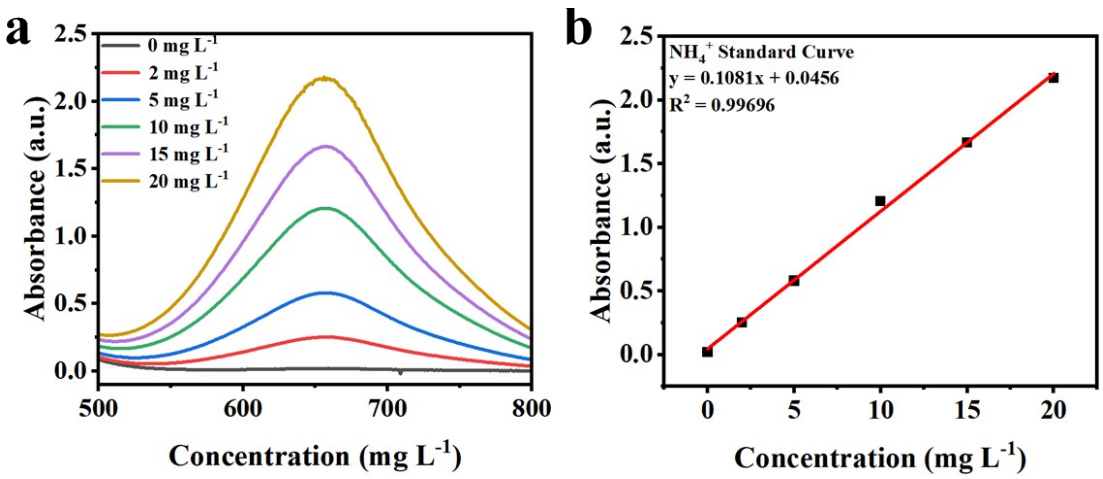

Fig. S11. a) The UV-Vis absorbance spectra and b) the corresponding calibration curve of absorbance versus concentration of NH_4^+.

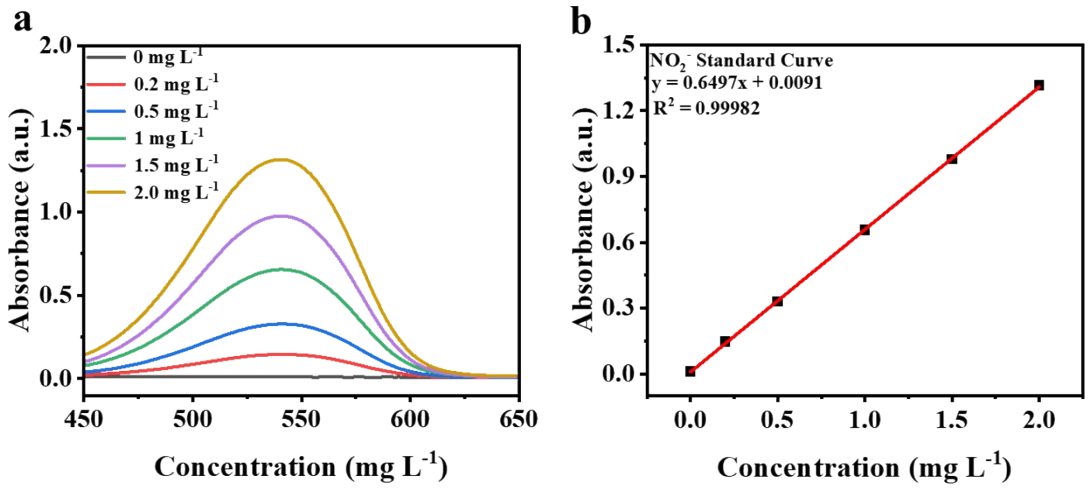

Fig. S12. a) The UV-Vis absorbance spectra and b) the corresponding calibration curve of absorbance versus concentration of NO_2^-.

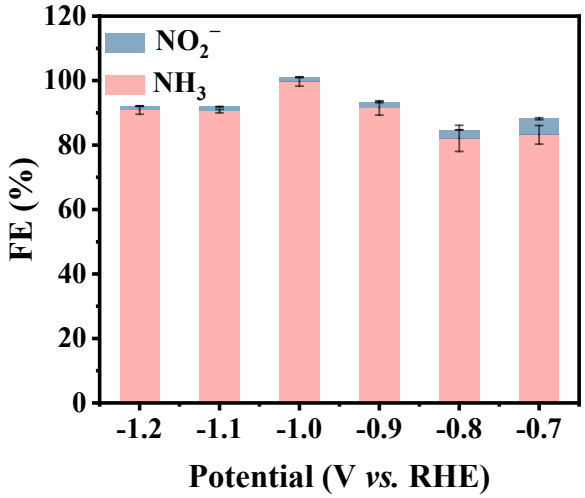

Fig. S13. FE-NH_3 and FE-NO_2^- of FeSA@CoO/Co_3O_4 NC.

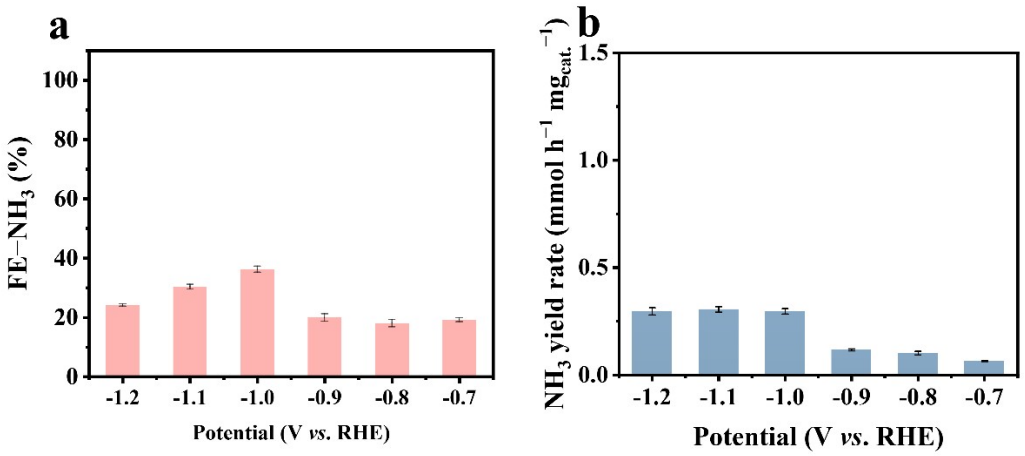

Fig. S14. a) FE-NH_3 and b) NH_3 yield rate of NC substrate under various applied potentials in 0.5 M Na_2SO_4 aqueous solution containing 0.1 M NO_3^-.

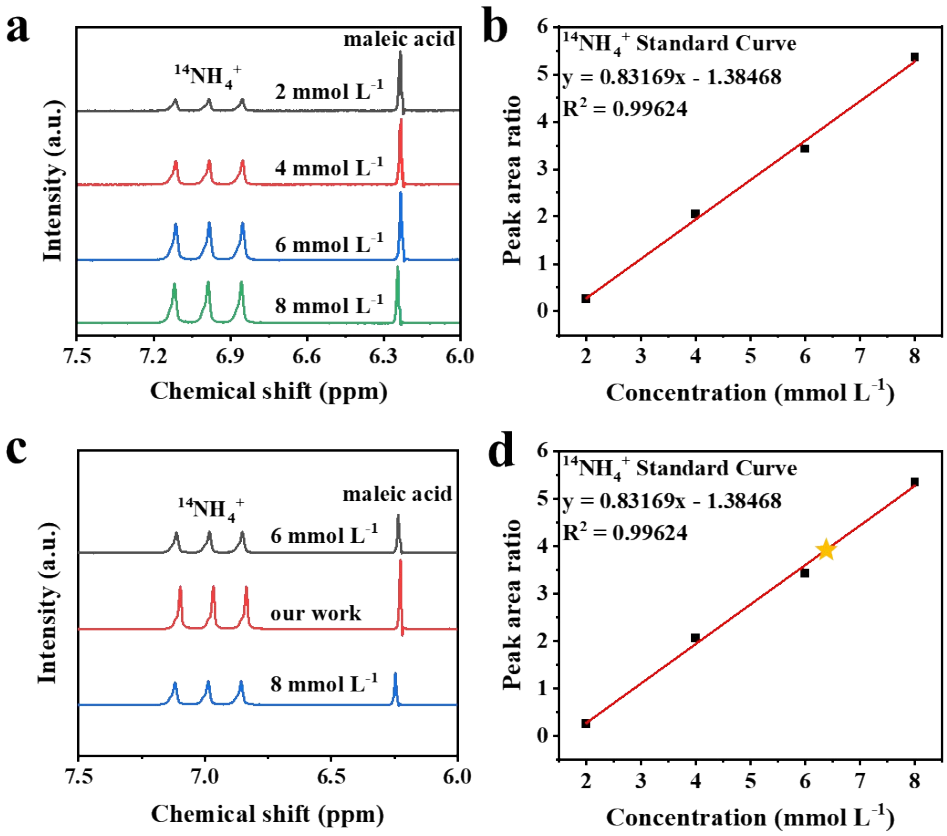

Fig. S15. a) ^{1}H-NMR spectra of various $^{14}NH_4^+$ concentrations using maleic acid as reference (50 ppm). b) Integral area ratio ($^{14}NH_4^+/C_4H_4O_4$) versus $^{14}NH_4^+$ concentration. c) ^{1}H-NMR spectra of the electrolyte after eNO_3RR using FeSA@CoO/Co_3O_4 NC at −1.0 V for 1 h. d) The $^{14}NH_4^+$ concentrations of electrolyte quantified by ^{1}H-NMR spectra using maleic acid (50 ppm) as reference.

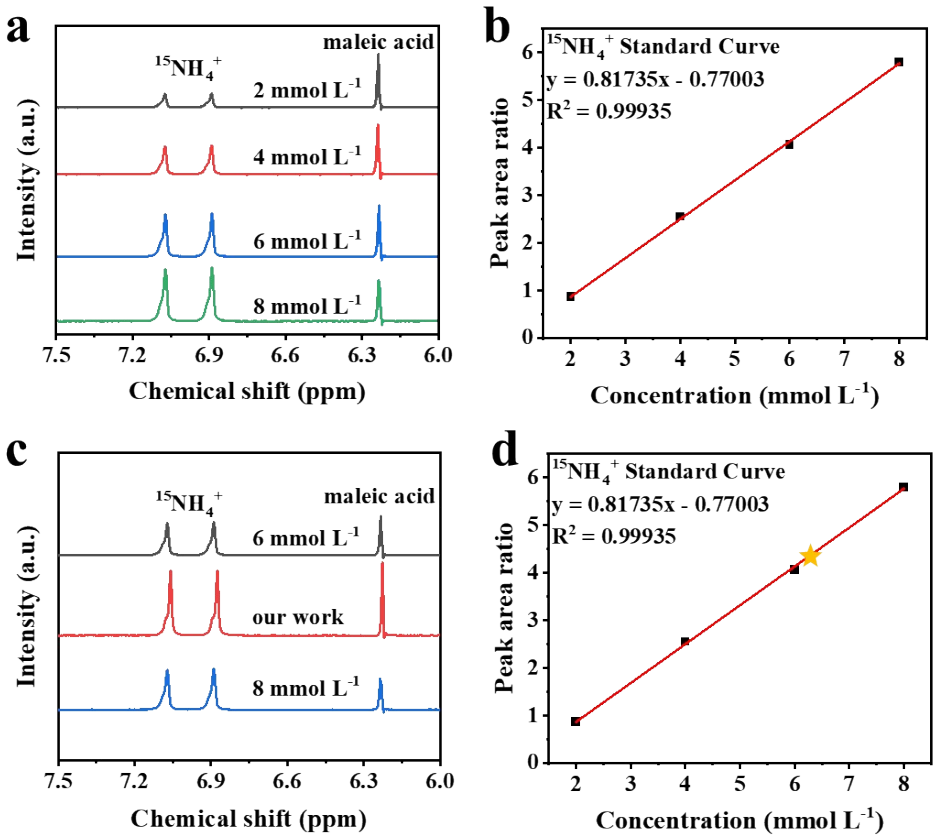

Fig. S16. a) ^{1}H-NMR spectra of various $^{15}NH_4^+$ concentrations using maleic acid as reference (50 ppm). b) Integral area ratio ($^{15}NH_4^+/C_4H_4O_4$) versus $^{15}NH_4^+$ concentration. c) ^{1}H-NMR spectra of the electrolyte after eNO_3RR using FeSA@CoO/Co_3O_4 NC at −1.0 V for 1 h. d) The $^{15}NH_4^+$ concentrations of electrolyte quantified by ^{1}H-NMR spectra using maleic acid (50 ppm) as reference.

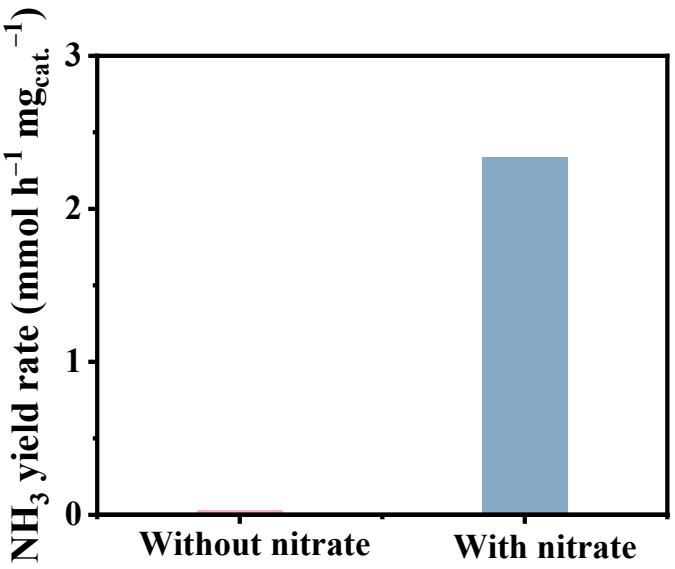

Fig. S17. NH_3 yield rate with or without NO_3^- at −1.0 V (*vs.* RHE).

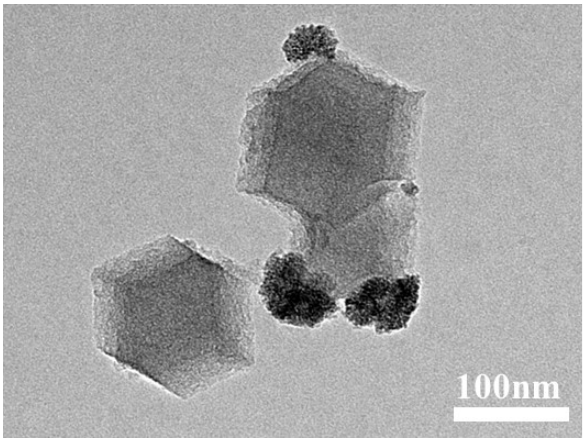

Fig. S18. TEM image of FeSA@CoO/Co_3O_4 NC after cycling test.

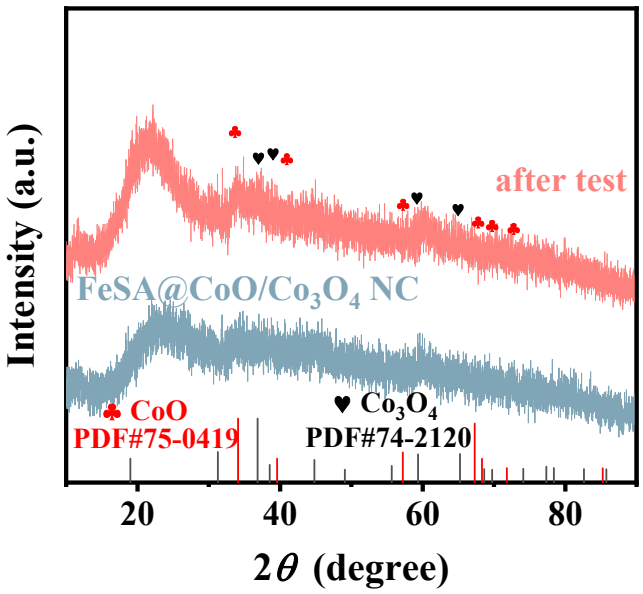

Fig. S19. XRD patterns of FeSA@CoO/Co_3O_4 NC after cycling test.

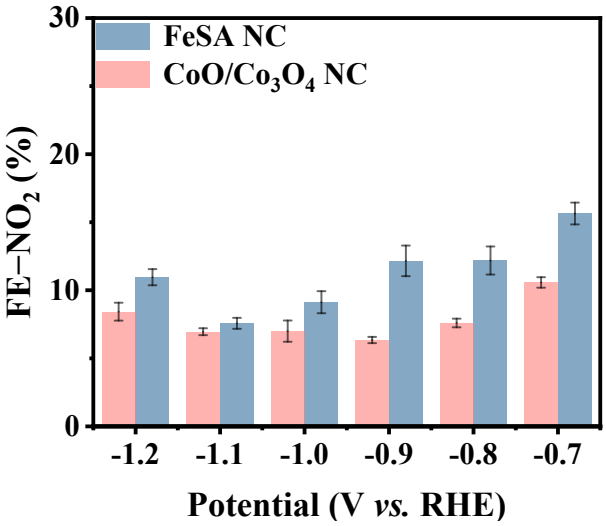

Fig. S20. FE-NO_2^- of a) FeSA NC and b) CoO/Co_3O_4 NC in 0.5 M Na_2SO_4 aqueous solution containing 0.1 M NO_3^-.

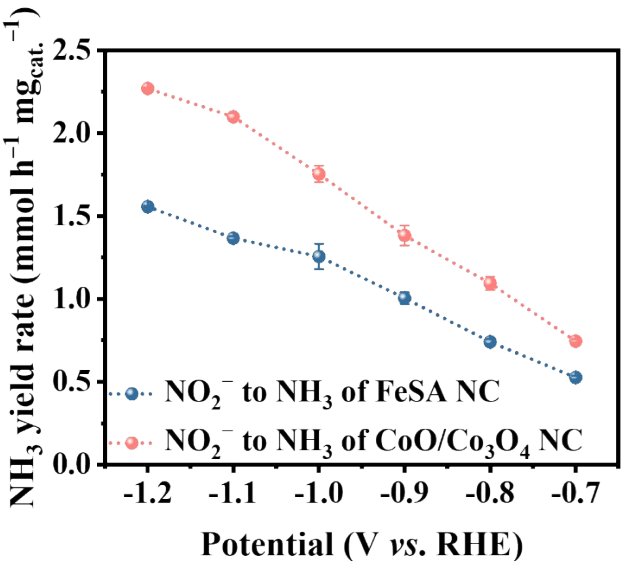

Fig. S21. NH_3 yield rate of FeSA NC and CoO/Co_3O_4 NC in 0.5 M Na_2SO_4 aqueous solution containing 0.1 M NO_2^-.

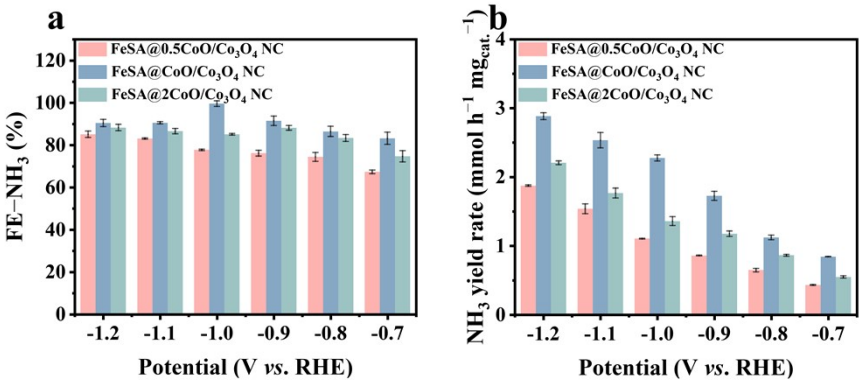

Fig. S22. (a) FE−NH_3 and (b) NH_3 yield rates of FeSA@0.5CoO/Co_3O_4 NC, FeSA@CoO/Co_3O_4 NC, and FeSA@2CoO/Co_3O_4 NC.

FeSA@*x*CoO/Co_3O_4 NC with different loading amount of CoO/Co_3O_4 were prepared via regulating the dosage of Co precursor: an experimental sample with an optimal Co precursor dosage, along with two control samples featuring Co precursor dosages of 0.5 and 2.0 times the experimental sample's dosage (designated as FeSA@0.5CoO/Co_3O_4 NC and FeSA@2CoO/Co_3O_4 NC, respectively). For the FeSA@0.5CoO/Co_3O_4 NC sample with the inadequate CoO/Co_3O_4 loading amount failed to realize effective deoxygenation and hydrogenation of NO_2^-. In contrast, the excessive CoO/Co_3O_4 in the FeSA@2CoO/Co_3O_4 NC sample fully covered the FeSA sites, thereby adsorption and activation of NO_3^-. Accordingly, the experimental sample FeSA@CoO/Co_3O_4 NC with a moderate proportion of FeSA to CoO/Co_3O_4 exhibited the optimal eNO_3RR performance.

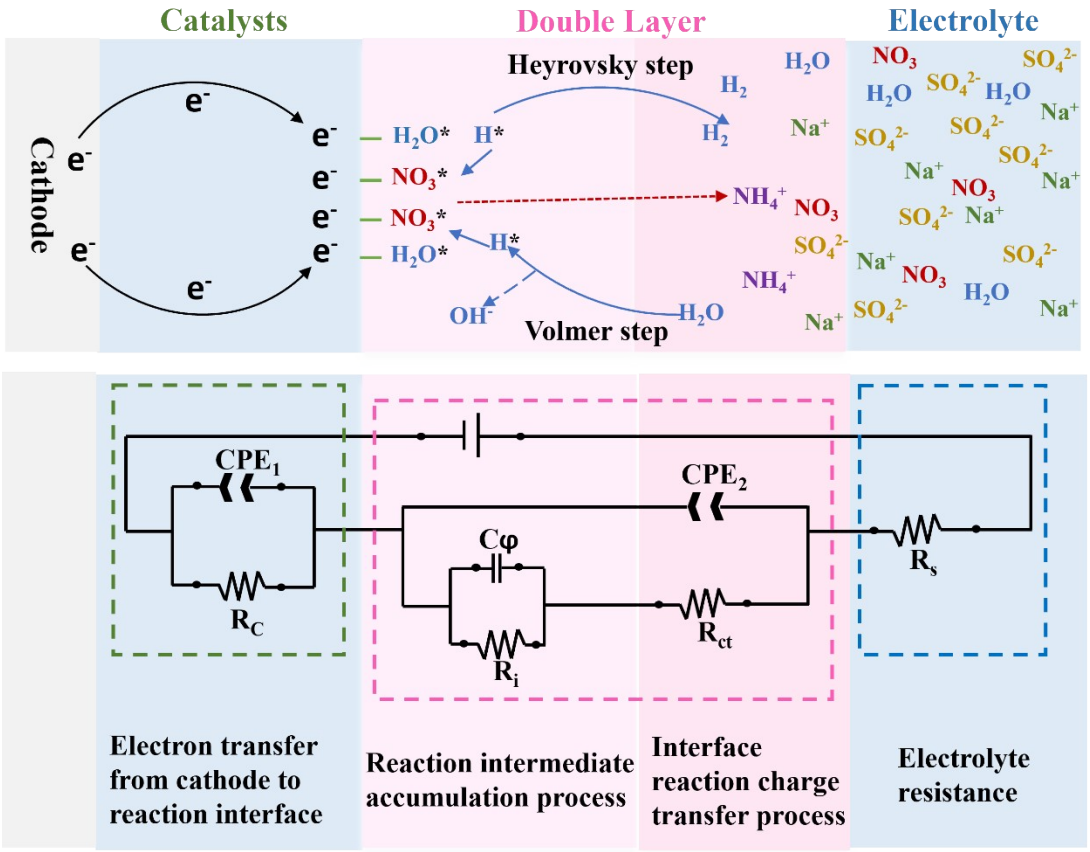

Fig. S23. Equivalent circuit model used in fitting the electrochemical impedance spectra and schematic diagram of the proposed reaction mechanism over FeSA@CoO/Co_3O_4 NC catalyst.

The cathodic resistance consists of four components: a) resistance (R_C) of electron transfer from the cathode to the catalytic sites; b) resistance (R_i) associated with the adsorption of intermediates at the reaction interface; c) resistance (R_{ct}) of charge transfer from the reaction interface to the intermediates, and d) diffusion resistance (R_S) of products in the electrolyte.[7]

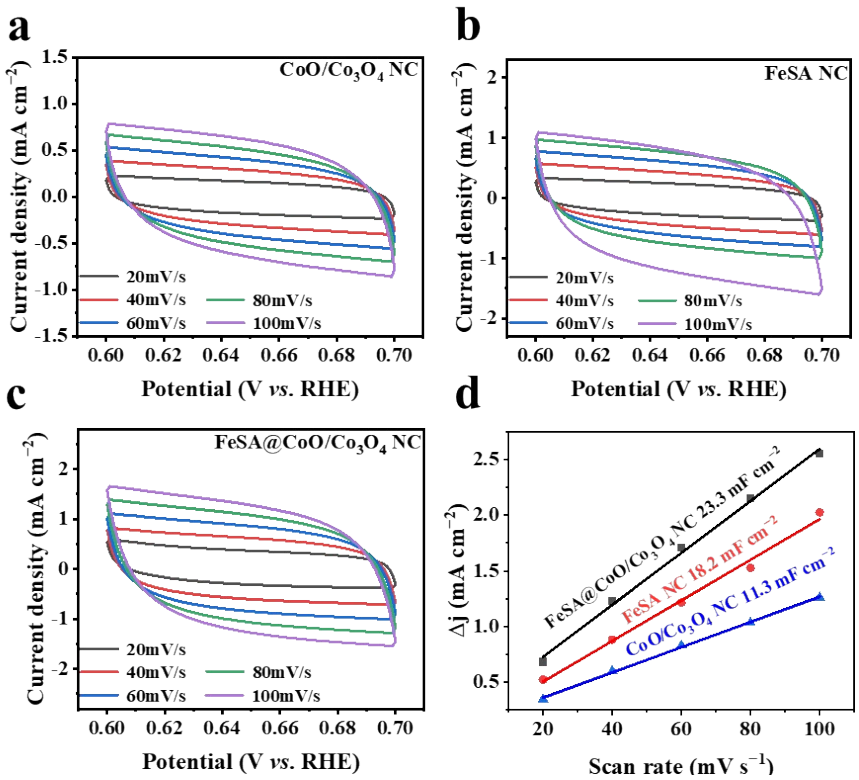

Fig. S24. CV curves in the double-layer region of a) CoO/Co_3O_4 NC, b) FeSA NC and c) FeSA@CoO/Co_3O_4 NC at different scan rates from 20 to 100 mV s^{-1}. d) Charging current density differences plotted against scan rates of FeSA@CoO/Co_3O_4 NC, FeSA NC, and CoO/Co_3O_4 NC.

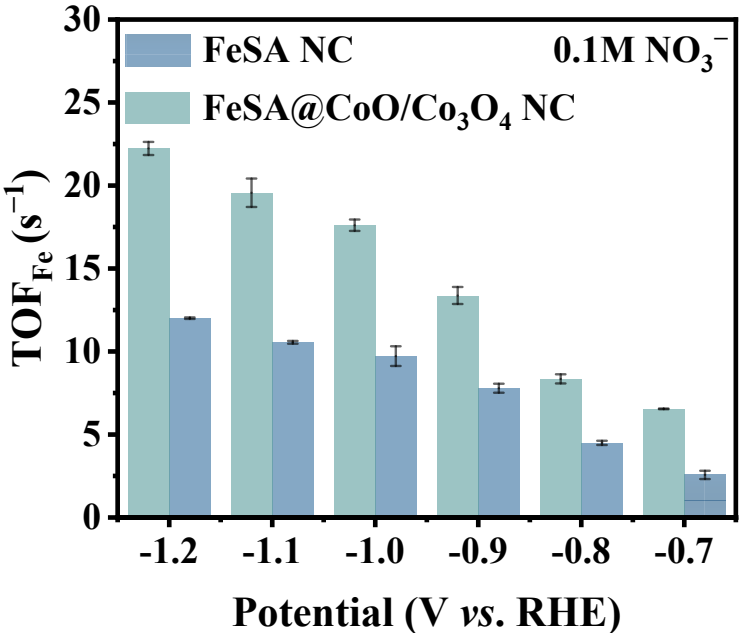

Fig. S25. Potential-dependent TOF values of FeSA NC and FeSA@CoO/Co_3O_4 NC.

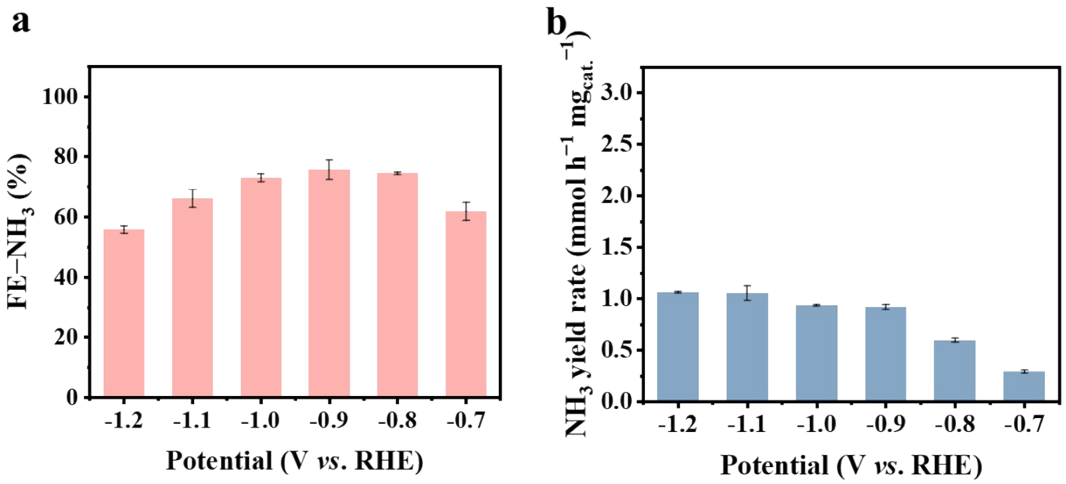

Fig. S26. eNO_3RR performance of physical mixture of FeSA NC and CoO/Co_3O_4 NC. a) FE-NH_3 and b) yield rate of NH_3 obtained from the physical mixture of FeSA NC and CoO/Co_3O_4 NC under various applied potentials in 0.1 M NO_3^- solution.

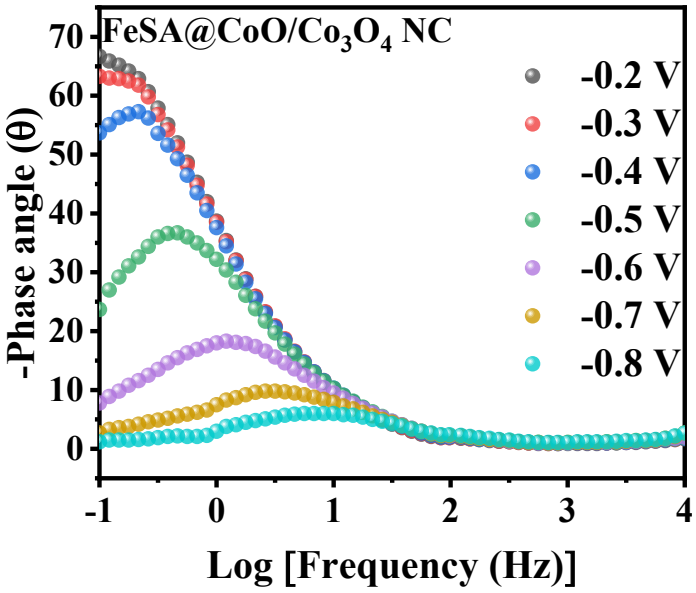

Fig. S27. Bode phase plots of FeSA@CoO/Co_3O_4 NC at various potentials in 0.5 M Na_2SO_4.

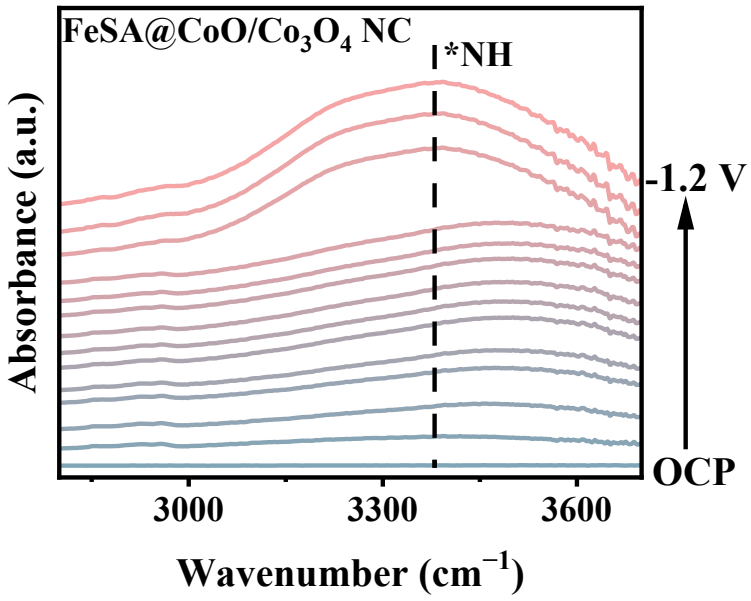

Fig. S28. In situ FTIR spectra of FeSA@CoO/Co_3O_4 NC.

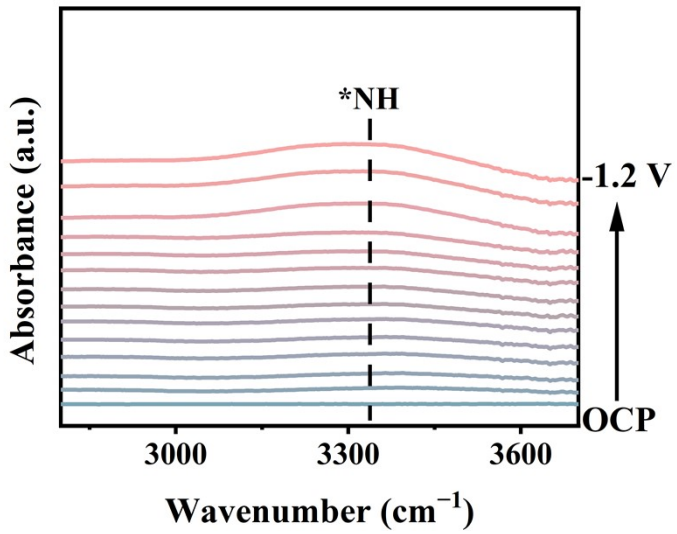

Fig. S29. In situ FTIR spectra of FeSA NC.

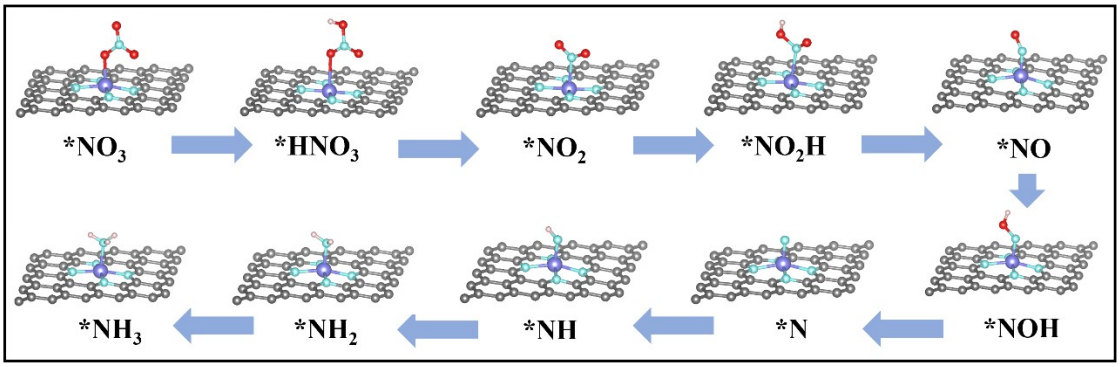

Fig. S30. Structural models of key intermediates on FeSA sites.

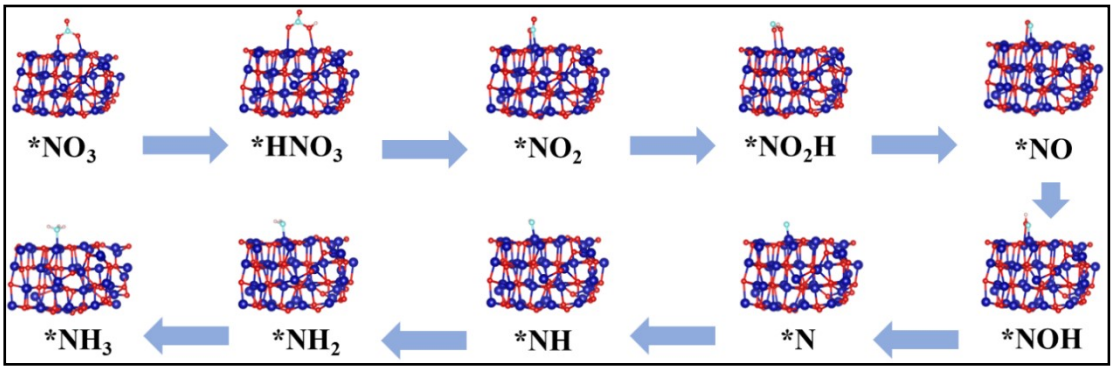

Fig. S31. Structural models of key intermediates on CoO/Co_3O_4 sites.

Supporting Tables

Table S1. Fe and Co contents of the catalysts based on ICP-MS analysis.

Catalyst	Fe content (wt%)	Co content (wt%)
FeSA NC	0.22	–
CoO/Co_3O_4 NC	–	3.25
FeSA@CoO/Co_3O_4 NC	0.20	3.00

Table S2. EXAFS data fitting results of FeSA@CoO/Co_3O_4 NC.

Catalyst	Shell	*CN*	*R* (Å)	σ^2	ΔE_0(eV)
FeSA@CoO/Co_3O_4 NC	Fe-N	3.91 ± 0.2	1.99 ± 0.05	0.0081	−1.7 ± 0.8

CN represents coordination number, R represents bond distance, σ^2 represents Debye-Waller factor, and ΔE_0 represents edge-energy shift.

Table S3. Comparison of the quantitative analysis between colorimetric method and ^{1}H-NMR for nitrate electroreduction at the optimal potential (−1.0 V *vs*. RHE)

Quantitative method	**N-source**	**Detected ion**	**NH_3 yield rate (mmol h^{-1} $mg_{cat.}^{-1}$)**	**Faradaic efficiency**
Colorimetric method	$Na^{14}NO_3$	$^{14}NH_4^+$	2.29	97.33
^{1}H-NMR			2.31	97.93
Colorimetric method	$Na^{15}NO_3$	$^{15}NH_4^+$	2.30	96.67
^{1}H-NMR			2.25	94.29

Table S4. Comparison of FE and yield rate of ammonia by eNO_3RR.

Catalysts	Electrolyte	FE-NH_3	NH_3 yield rate (mmol h^{-1} $mgcat.^{-1}$)	Ref.
FeSA@CoO/Co_3O_4 NC	0.5 M Na_2SO_4 + 0.1 M $NaNO_3$	99.6%	2.28	This work
$PdCu_2O$ CEO	0.1 M K_2SO_4 + 50 ppm KNO_3	96.56%	0.054	8
Fe SAC	0.1 M K_2SO_4 + 0.5 M KNO_3	75 %	1.17	9
FE-N/P-C	0.1 M KOH + 0.1 M KNO_3	90.3%	1.05	10
CuCoAl LDH	0.5 M Na_2SO_4 + 0.05 M KNO_3	99.5%	0.22	11
Cu-Co_3O_4	0.1 M Na_2SO_4 + 0.05 M $NaNO_3$	86.5%	0.036	12
$Cu_{50}Co_{50}$	1 M KOH + 100 mM NO_3^-	100 ± 1%	0.96	13
Fe_1/NC-900	0.1 M K_2SO_4 + 0.5 M KNO_3	86.7%	0.35	14
Co_1-P/NPG	0.5 M K_2SO_4 + 0.1 M KNO_3	93.8%	0.505	15
Fe/Cu-NG	1 M KOH + 0.1 M KNO_3	92.51%	1.08	16

References:

1. D. Zhu, L. Zhang, R. E. Ruther and R. J. Hamers, *Nat. Mater.*, 2013, **12**, 836-841.
2. G. Kresse and J. Hafner, *Phys. Rev. B*, 1993, **47**, 558-561.
3. G. Kresse and J. Hafner, *Phys. Rev. B*, 1994, **49**, 14251-14269.
4. J. P. Perdew, K. Burke and M. Ernzerhof, *Phys. Rev. Lett.*, 1996, **77**, 3865-3868.
5. G. Kresse and D. Joubert, *Phys. Rev. B*, 1999, **59**, 1758-1775.
6. S. Grimme, J. Antony, S. Ehrlich and H. Krieg, *J. Chem. Phys.*, 2010, **132**, 154104.
7. S. Liang, X. Teng, H. Xu, L. Chen and J. Shi, *Angew. Chem. Int. Ed.*, 2024, **63**, e202400206.
8. Y. Xu, K. Ren, T. Ren, M. Wang, Z. Wang, X. Li, L. Wang and H. Wang, *Appl. Catal., B*, 2022, **306**, 121094.
9. Z.-Y. Wu, M. Karamad, X. Yong, Q. Huang, D. A. Cullen, P. Zhu, C. Xia, Q. Xiao, M. Shakouri, F.-Y. Chen, J. Y. Kim, Y. Xia, K. Heck, Y. Hu, M. S. Wong, Q. Li, I. Gates, S. Siahrostami and H. Wang, *Nat. Commun.*, 2021, **12**, 2870.
10. Z. Fang, Z. Jin, S. Tang, P. Li, P. Wu and G. Yu, *ACS Nano*, 2022, **16**, 1072-1081.
11. W. Wang, J. Chen and E. C. M. Tse, *J. Am. Chem. Soc.*, 2023, **145**, 26678-26687.
12. Z. Niu, S. Fan, X. Li, Z. Liu, J. Wang, J. Duan, M. O. Tadé and S. Liu, *ACS Catal.*, 2022, **14**, 35477-35484.
13. J.-Y. Fang, Q.-Z. Zheng, Y.-Y. Lou, K.-M. Zhao, S.-N. Hu, G. Li, O. Akdim, X.-Y. Huang and S.-G. Sun, *Nat. Commun.*, 2022, **13**, 7899.
14. L. Liu, T. Xiao, H. Fu, Z. Chen, X. Qu and S. Zheng, *Appl. Catal., B*, 2023, 323.
15. J. Ni, J. Yan, F. Li, H. Qi, Q. Xu, C. Su, L. Sun, H. Sun, J. Ding and B. Liu, *Adv. Energy Mater.*, 2024, **14**, 2400065.
16. S. Zhang, J. Wu, M. Zheng, X. Jin, Z. Shen, Z. Li, Y. Wang, Q. Wang, X. Wang, H. Wei, J. Zhang, P. Wang, S. Zhang, L. Yu, L. Dong, Q. Zhu, H. Zhang and J. Lu, *Nat. Commun.*, 2023, **14**, 3634.